Analytical Methods

RSC Publishing

PAPER

View Article Online
View Journal | View Issue



Cite this: *Anal. Methods*, 2013, **5**, 5929

# Highly luminescent glutathione-capped ZnS : Mn/ZnS core/shell doped quantum dots for targeted mannosyl groups expression on the cell surface†

Rui Ban,[ab] Jingjing Li,[ac] Juntao Cao,[a] Penghui Zhang,[a] Jianrong Zhang*[a] and Jun-jie Zhu*[a]

Received 16th July 2013
Accepted 20th August 2013

DOI: 10.1039/c3ay41189c

www.rsc.org/methods

High-quality glutathione (GSH) capped ZnS : Mn/ZnS core/shell doped quantum dots (d-dots) with pure dopant emission band and excellent stability have been synthesized directly in aqueous media. The influences of experimental variables on the luminescent properties of the ZnS : Mn/ZnS nanocrystals have been investigated. The quantum yield of the dopant Mn photoluminescence in the as-prepared ZnS : Mn/ZnS core/shell d-dots can be up to 27.4%. The value is the highest reported to date for ZnS : Mn d-dots *via* the direct aqueous synthetic method. Their optical features and structure have been characterized by UV-Visible spectroscopy, photoluminescence (PL) spectroscopy, transmission electron microscopy (TEM) and X-ray diffraction (XRD) in detail. Additionally, the stability study against UV irradiation indicated that the obtained d-dots possess excellent photostability. Furthermore, the MTT assay demonstrated that the ZnS : Mn QDs do not exhibit any cytotoxicity toward HeLa cells up to a concentration of 600 μg $mL^{-1}$. Using the Con A-mannose recognition system as a model, Con A functionalized ZnS : Mn/ZnS nanocrystals were prepared and successfully used for targeted mannosyl groups expression on the HeLa cells surface. Our investigation clearly shows that the GSH capped ZnS : Mn QDs are promising candidates as biological fluorescent labels.

## Introduction

Semiconductor nanocrystals (NCs), otherwise known as quantum dots (QDs), have attracted considerable interest over the past decades due to their potential applications in biomedical labeling, fluorescent biosensors, optoelectronics, and solar cells, *etc.*[1–7] The most investigated quantum dots are often cadmium-based materials, which have well developed synthetic chemistry and widely documented physical properties.[8–14] However, these NCs are not suitable generally for applications in the biological area due to their containing the heavy metal, Cd, which can cause toxicity.[15] Considering the inherent problems of heavy metal-containing QDs and to broaden their applications in biological and medical fields, the search for alternative probes has become one of the most challenging domains. It has been demonstrated that doping semiconductor NCs are being explored as viable alternatives to undoped NCs with additional advantages, such as larger Stokes shift to avoid self-absorption, longer excited state lifetime, enhanced thermal and chemical stabilities, and minimized toxicity. Of these, Mn-doped semiconductor NCs have been regarded as a promising new generation of luminescent NCs.[16–18] Owing to the potential high photoluminescence (PL) quantum yield (QY) from the $Mn^{2+}$ $^4T_1$ to $^6A_1$ transition, a sustained effort to enhance the dopant emission intensity from doped NCs such as ZnS, ZnSe, and CdS hosts has lasted for more than a decade.[19–28] Particularly, ZnS : Mn d-dots, which are free of Cd and Se, are greener materials and have become popular nanophosphors for electroluminescent devices. Additionally, the luminescent lifetime of ZnS : Mn d-dots NCs reaches *ca.* 1 ms. Such a long lifetime enables the luminescence from the nanocrystal to be readily distinguished from the background luminescence with a very short lifetime.[29,30] These advantages make them ideal candidates as fluorescent labeling agents, especially in biology.

In the past decade, some synthetic approaches have been developed to produce ZnS : Mn d-dots, mostly focused on two main methods.[25,31–41] The first method is organic-phase growth, which can produce high quality ZnS : Mn d-dots with high QY, good crystallinity and monodispersity. However, unavoidable hazardous organic reagents in the synthesis, long reaction time and limited operation conditions confined their utility. Additionally, the hydrophobic properties of the as-prepared d-dots further limited their applications in biological domains. So for

[a]*State Key Laboratory of Analytical Chemistry for Life Science, School of Chemistry and Chemical Engineering, Nanjing University, Nanjing 210093, P.R. China. E-mail: jrzhang@nju.edu.cn; jjzhu@nju.edu.cn; Fax: +86 25 83317761; Tel: +86 25 83686130*
[b]*School of Chemistry and Environmental Science, Guizhou Minzu University, Guiyang 550025, P.R. China*
[c]*School of Medical Imaging, Xuzhou Medical College, Xuzhou 221000, P.R. China*

† Electronic supplementary information (ESI) available. See DOI: 10.1039/c3ay41189c

water-soluble and biocompatible NCs, the exchange of the hydrophobic ligands with hydrophilic ligands, such as thioacids, and subsequent transfer of QDs from oil to aqueous solution is necessary. However, the QY and stability of the NCs are significantly reduced after this step. The second method is the direct aqueous synthetic method, which has been proven to be simpler, cheaper and less toxic to prepare water-soluble ZnS : Mn d-dots. However, the d-dots synthesized by this method usually suffer from poor crystallinity and low QY.[32] 3-Mercaptopropionic acid (MPA), the common stabilizer in this system, is a volatile liquid with odor and carcinogenicity, which excludes it from green chemistry. Furthermore, the dual emissions of the obtained d-dots, band edge emission and dopant emission coming from the partial doping of $Mn^{2+}$ ions into the host materials, limits their applications in certain fields. Recently, Schneider group have developed an approach to synthesize thioglycerol-capped ZnS : Mn QDs with pure dopant emission,[42] whereas the PL QY was 13.2% in this strategy. Moreover, an efficient strategy to improve the PL QY and stability of the QDs is to deposit an inorganic shell with a higher band gap around the cores, resulting in the formation of the core/shell nanostructure. For example, improved fluorescence properties have been observed in several core/shell nanoparticles, such as ZnS : Mn/ZnS,[25,26,28,32,33,43] ZnS : Mn/ZnO,[44] ZnS : Mn/$SiO_2$[45] and ZnS : Mn/$Zn(OH)_2$.[46] Therefore, it is still necessary to find a safer and more environment-friendly stabilizer to realize the direct aqueous synthesis of ZnS : Mn d-dots and their core/shell structure with pure dopant emission and good stability.

In this paper, we induced the thiol ligand glutathione (GSH) as the stabilizer, which is known as a natural tripeptide consisting of glutamic acid, cysteine and glycine. Due to excellent biocompatibility, high stability, non-volatilization, its lack of odour and the environmental-friendliness of GSH, it has been widely adopted to synthesize highly fluorescent metal nanoparticles.[10,47–49] Herein, we described a facile route for the preparation of highly luminescent GSH capped ZnS : Mn/ZnS core/shell doped quantum dots in aqueous solution. The synthesis is based on a two-step approach: (i) synthesis of ZnS : Mn d-dots and (ii) depositing ZnS shell on the ZnS : Mn core in the aqueous solution. Consequently, the obtained water-soluble ZnS : Mn/ZnS d-dots with pure dopant emission own less surface defects and high PL QY (with the highest QY of 27.4%). To the best of our knowledge, it is the first report GSH capped ZnS : Mn/ZnS d-dots with pure dopant emission *via* direct aqueous synthetic method. In addition, a white powder of ZnS : Mn/ZnS d-dots with high fluorescence could be obtained and was found to be stable for at least one year. Remarkably, the ZnS : Mn/ZnS d-dots possessed excellent optical stability and biocompatibility. Furthermore, Con A, a lectin of carbohydrate-binding protein,[50] was linked to the ZnS : Mn/ZnS d-dots as a fluorescence probe to profile the mannosyl groups expression on HeLa cells by laser scanning confocal microscopy.

## Experimental section

### Chemicals

Glutathione (GSH, 99%), mercaptopropionic acid (MPA, 99%), L-cysteine (L-cys, 99%), and mercaptoethylamine (99%) were supplied from Aladdin Reagent Company. $ZnSO_4$ (99%), $MnCl_2$ (99%) and $Na_2S$ (99%) were obtained from Shanghai Reagent Company. Ethanol ($CH_3CH_2OH$, anhydrous) was of analytical grade and used without further purification. Other chemicals were of analytical grade. Phosphate buffer solution (PBS, 20 mM, pH = 8.0) was prepared by mixing the solutions of $K_2HPO_4$ and $NaH_2PO_4$. 3-(4,5-Dimethylthiazol-2-yl)-2,5-diphenyltetrazolium bromide (MTT), concanvalin A (Con A), mannose, 1-ethyl-3-(3-dimethylaminopropyl)carbodiimide hydrochloride (EDC), and *N*-hydroxysuccinimide (NHS) were purchased from Sigma (St. Louis, MO, USA). Ultrapure water with 18.2 MΩ (Millipore Simplicity, USA) was used in the experiments.

### Characterization

Fluorescence measurements were performed using a Shimadzu RF-5301 PC fluorescence spectrometer. UV-vis absorption spectra were obtained by a UV-3600 spectrophotometer (Shimadzu). Samples for transmission electron microscopy (TEM) and high-resolution TEM (HRTEM) were prepared by dropping the samples dispersed in water onto carbon-coated copper grids with the excess solvent evaporated. TEM images and HRTEM images were recorded on a Shimadzu JEM-2010 CX with an accelerating voltage of 100 kV and on a JEM-2010 F with an accelerating voltage of 200 kV, respectively. X-ray diffraction (XRD) measurements were performed on a Shimadzu XRD-6000 powder X-ray diffractometer, using Cu Kα ($\lambda$ = 1.5405 Å) as the incident radiation. The fluorescence lifetime of the ZnS : Mn d-dots was measured with a FLS 920 time-resolved spectroscope (Edinburgh). Inductively coupled plasma atomic emission spectroscopy (ICP-AES) was carried out with a Perkin-Elmer Optima 3000 DV after dissolving the aqueous ZnS : Mn d-dots in 5% hydrochloric acid. Electron paramagnetic resonance (EPR) measurements were performed using an X-band (9.7747 GHz) EMX-10/12 spectrometer (Bruker) at room temperature. The PL QY of the ZnS : Mn d-dots samples were determined following the procedure in ref. 26 by using fluorescent dye quinine sulfate (see ESI, Fig. S1†) as a reference standard.[51,52] *In vitro* cytotoxicity of the QDs was assessed using the MTT assay and the absorbance was measured at 490 nm using the Multiskan Ascent (Thermo Labsystems, Franklin, MA, USA). The cell images were obtained with a Leica TCS SP5 confocal microscope. All of the experiments were carried out at room temperature except the photostability measurement of the ZnS : Mn d-dots at 37 °C.

### Synthesis of GSH-capped ZnS : Mn d-dots in aqueous media

The preparation of GSH-capped ZnS : Mn d-dots was performed according to previous reports with some adaptations.[31] In a typical experiment, 2.5 mL of 0.1 M $ZnSO_4$, 1 mL of 0.01 M $MnCl_2$, 5 mL of 0.1 M GSH and 41.5 mL water were mixed together. The pH of the mixture was adjusted to 11.0 with 1 M NaOH. After the purging of air by $N_2$ bubbling for 30 min, 0.25 mmol $Na_2S$ was quickly injected into the solution. The mixture was stirred for another 20 min, and then the solution was aged at 50 °C under air for 2 h to form GSH-capped ZnS : Mn d-dots. The ZnS : Mn d-dots could be precipitated by ethanol. After centrifugation and washing with ethanol, the precipitate was then dried in vacuum.

 

### Synthesis of water-soluble ZnS : Mn/ZnS core/shell d-dots

The ZnS : Mn/ZnS precursor solution was prepared by adding the as-prepared ZnS : Mn d-dots to a solution containing 5.0 mM $ZnSO_4$ and 12 mM GSH. After adjusting the pH value to 11.0 with 1 M NaOH, the precursor solution was saturated with $N_2$ by bubbling for 1 h, followed by the addition of 5.0 mM of $Na_2S$. The mixture in a 100 mL round-bottom flask equipped with a stirrer, a $N_2$ gas inlet, and a condenser, was heated to 70 °C and 1 h later, ZnS : Mn/ZnS core/shell d-dots could be obtained. After cooling down to room temperature (~22 °C), the ZnS : Mn/ZnS core/shell d-dots were purified by centrifugation and decantation with the addition of ethanol. The ZnS : Mn/ZnS core/shell d-dots were further washed with ethanol and finally dried under vacuum at room temperature. The obtained powder was highly soluble in water and could be used for XRD and ICP measurement.

### Preparation of the ZnS : Mn/ZnS QDs-Con A probe

Con A was conjugated with ZnS : Mn/ZnS QDs *via* an EDC/NHS-mediated reaction. First, 100 μL of 1 mg $mL^{-1}$ ZnS : Mn/ZnS QDs solution was added into 800 μL PBS solution of pH 7.4 containing 2 mM EDC and 5 mM NHS, and the mixture was incubated for 30 min at room temperature. Then 100 μL of Con A (1 mg $mL^{-1}$) was added to this mixture and reacted for 12 h at 4 °C. The ZnS : Mn/ZnS QDs-Con A conjugates were ultra-filtrated using Millipore filtration tube (3 kDa) at 8000 g for 30 min at 4 °C to remove the non-conjugated ZnS : Mn/ZnS QDs and by-product. The concentrated QDs-Con A conjugates were dispersed in 100 μL PBS solution of pH 7.4. For cell staining experiments, 100 μL of the resultant ZnS : Mn/ZnS QDs-Con A was diluted with 900 μL Tris–HCl (0.1 mM, pH 7.4) containing 0.1 mM $Ca^{2+}$ and 0.1 mM $Mn^{2+}$.

### Cytotoxicity assay

The cytotoxicity of as-prepared QDs was evaluated by the MTT assay on human cervical carcinoma HeLa cells and the procedure was carried out according to the literature reported previously.[53] Briefly, HeLa cells were seeded in 96-well plates at $5 \times 10^3$ cells per well in DMEM medium and incubated at 37 °C in a humidified atmosphere with 5% $CO_2$ for 12 h. The cells were then incubated in triplicate with grade concentrations of CdTe QDs,[54] ZnS : Mn cores and ZnS : Mn/ZnS core/shell d-dots at 37 °C for 24 h or 48 h, respectively. After removing the medium and washing the cells twice with PBS buffer, DMEM containing MTT (5 mg $mL^{-1}$) was added to each well and further incubated with the cells for another 4 h. Then the medium containing MTT was replaced by 150 μL of DMSO to solubilize the formazan crystals precipitate. The absorbance of the purple formazan was recorded at 490 nm using an ELISA plate reader. The cytotoxicity results were calculated based on the data of three replicate tests.

### Confocal fluorescence imaging for the mannosyl group

HeLa cells ($5 \times 10^3$ cells per mL) were seeded in microplate wells and incubated for 4 h under the same conditions as those for cell culture. After the culture solution was removed, the microplate wells were blocked with 1% BSA for 30 min. After the cells were washed thrice with pH 7.4 PBS, the cells were incubated with 50 μL of ZnS : Mn/ZnS QDs-Con A probe solution. After the specific conjugation between ZnS : Mn/ZnS QDs-Con A probe and mannosyl groups on cells for 60 min at 37 °C, the microplate wells were washed thrice with PBS to remove the non-conjugated ZnS : Mn/ZnS QDs-Con A probe. A Leica TCS SP5 confocal microscope (LSCM) was used to image the HeLa cells surface mannosyl groups. ZnS : Mn/ZnS QD fluorescence was detected using UV excitation and 550–640 nm emission filters. For control experiments, ZnS : Mn/ZnS QDs and ZnS : Mn/ZnS QDs-Con A-mannose were carried out by the same procedure.

## Results and discussion

### Characterization of the ZnS : Mn/ZnS core/shell d-dots

A two-step approach was adopted for preparation of ZnS : Mn/ZnS core/shell d-dots with pure dopant emission (Fig. 1). GSH-caped ZnS : Mn core were first prepared using a mixture of the dopant and the host precursor, and then the ZnS : Mn cores were coated with ZnS shell in aqueous solution through a precipitation reaction.

The optical properties of ZnS : Mn d-dots before and after the growth of the shell were monitored using UV-vis absorption and photoluminescence emission spectra (Fig. 2A). Similar to the UV-vis spectra, the excitation onset of the ZnS : Mn d-dots also shifts to lower energy with increased particle size. The ZnS : Mn d-dots were colourless in solution and white powders by precipitating with ethanol and drying under visible light (inset of Fig. 2A, top row). They emitted intense orange luminescence in both solution and solid state under UV light (inset of Fig. 2A, bottom row). A strong PL band is observed at about 580 nm, which is ascribed to the $Mn^{2+}$ ion $^4T_1$ to $^6A_1$ transition (Fig. 2B) and enhanced significantly after the growth of the ZnS shell. Compared with that of the previously reported ZnS : Mn d-dots in aqueous-phase synthetic method (Table S1†),[32,42,55] the defect related emission originating from the band-gap transition of ZnS was greatly suppressed in our case. Thus, the pure dopant emission of ZnS : Mn d-dots was obtained. Although thioglycerol-capped ZnS : Mn d-dots with the pure dopant emission have been reported recently, the long reaction time (up to 20 h) was required in this method. However, we drastically shortened the required time for sample preparation.[42] The QY of ZnS : Mn d-dots in aqueous solutions before and after the shell growth were determined to be 20.1% and 27.4% respectively, which were much higher than the QY of the ZnS : Mn d-

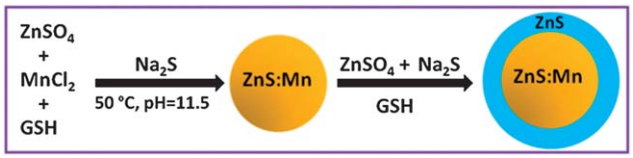


**Fig. 1** Schematic illustration of the synthesis of water-soluble ZnS : Mn/ZnS core/shell d-dots.

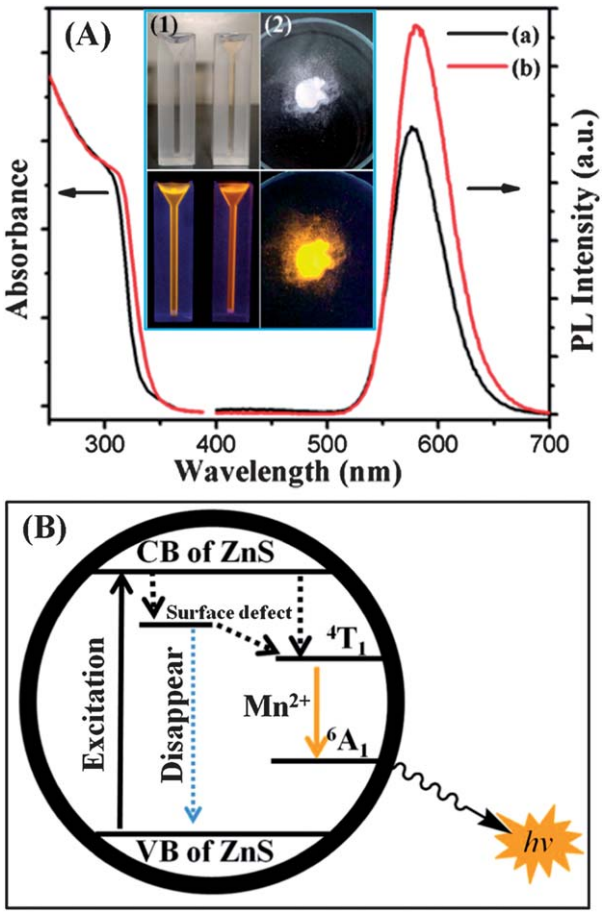


**Fig. 2** (A) Optical absorption (left line), and PL emission (right line) after excitation at 310 nm of GSH-capped ZnS : Mn d-dots (a) and ZnS : Mn/ZnS core/shell d-dots (b). The insets are photographs of ZnS : Mn d-dots (left) and ZnS : Mn/ZnS core/shell d-dots (right) in water (1) and ZnS : Mn/ZnS core/shell d-dots white powder (2) under visible (top row) and UV light (bottom row). (B) Schematic illustration of the emission levels of ZnS : Mn d-dots.

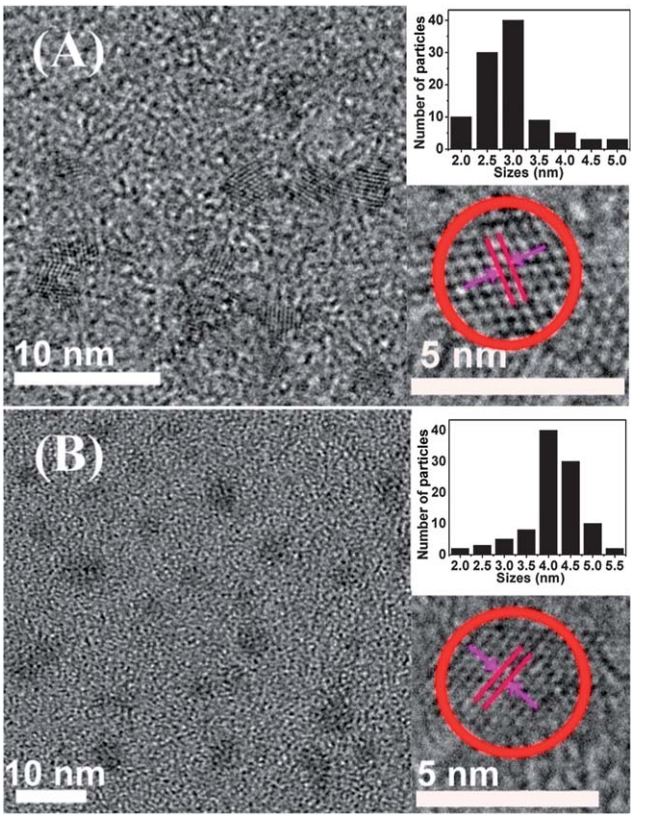


**Fig. 3** TEM micrograph and the corresponding particle size distribution of (A) ZnS : Mn cores, and (B) ZnS : Mn/ZnS core/shell d-dots.

dots that had been reported by other aqueous-phase synthetic methods.[32,42,55]

Fig. 3 shows the TEM results of the ZnS : Mn cores and the ZnS : Mn/ZnS core/shell d-dots. Nearly monodispersed core/shell d-dots were obtained with an average diameter of 4.2 nm. Compared to the core size (3.1 nm), the core/shell particle size was increased about 1.1 nm. The HRTEM image of the ZnS : Mn/ZnS core/shell d-dots shows the interplanar distance of 0.33 nm, which agreed well with that of 0.33 nm for the ZnS : Mn core nanocrystal. However, due to the similar electron densities and lattice parameter of the ZnS : Mn core and the ZnS shell, the contrast of the HRTEM image was unable to distinguish the shell and the core. Furthermore, Energy Dispersive Spectroscopy spectrum (Fig. S2†) of the ZnS : Mn/ZnS d-dots clearly showed the presence of S, Zn, Mn and O, in agreement with the element mapping analysis (Fig. S3†). The results further supported the conclusion that $Mn^{2+}$ ions were incorporated by substitution into the ZnS host lattice.

The X-ray diffraction patterns of the ZnS : Mn cores and the ZnS : Mn/ZnS core/shell d-dots are shown in Fig. 4A. The three main peaks located at 28.7°, 48.1°, and 56.4° correspond to the (111), (220), and (311) planes of zinc blende phase ZnS, respectively, which match well with the standard card (JCPDS no. 77-2100). It can be observed that these peaks are broadened when compared with bulk ZnS, confirming the nanocrystalline nature of all the samples. The average crystallite sizes of ZnS : Mn cores and ZnS : Mn/ZnS core/shell d-dots were estimated to be 3.1 and 4.2 nm from the XRD data, which kept accordance with the results obtained from TEM analysis.

The fluorescence lifetime of ZnS : Mn cores and the ZnS : Mn/ZnS core/shell d-dots at the emission of 580 nm are 2 ms and 3 ms, respectively (Fig. 4B). This is consistent with the values in previous reports.[34,35] The long fluorescence lifetime attributes to the emission of the single isolated $Mn^{2+}$ ions in a cubic site. The enhancement observed for ZnS : Mn/ZnS d-dots is a direct consequence of the deeper embedding of $Mn^{2+}$ emission centers in the NCs and of their increased isolation from the surface defects.

As shown in Fig. S4,† IR spectra were recorded to illustrate the existence of GSH on the surface of the prepared ZnS : Mn/ZnS core/shell d-dots. The IR absorption bands of free GSH at around 1600–1631 $cm^{-1}$ ($\upsilon_s$ $COO^-$) and 1403 $cm^{-1}$ ($\upsilon_m$ $COO^-$) are ascribed to –COO groups, whereas the peak 2524 $cm^{-1}$ ($\upsilon_m$ S–H) are assigned to –SH groups. By contrast, the disappearance of the S–H stretching vibrational peak in the IR spectrum of GSH-capped ZnS : Mn/ZnS core/shell d-dots indicated that the thiol group of GSH had combined onto the

 

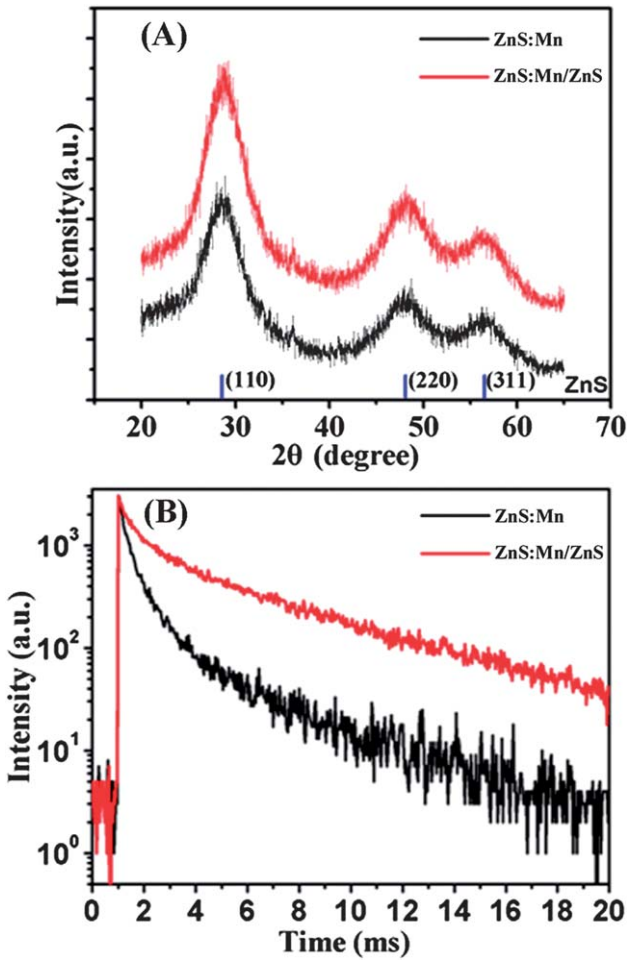


**Fig. 4** (A) XRD peak patterns for ZnS : Mn cores and the ZnS : Mn/Zn core/shell d-dots. (B) The PL decay curves for ZnS : Mn cores and the ZnS : Mn/Zn core/shell d-dots. Excitation wavelength: 310 nm.

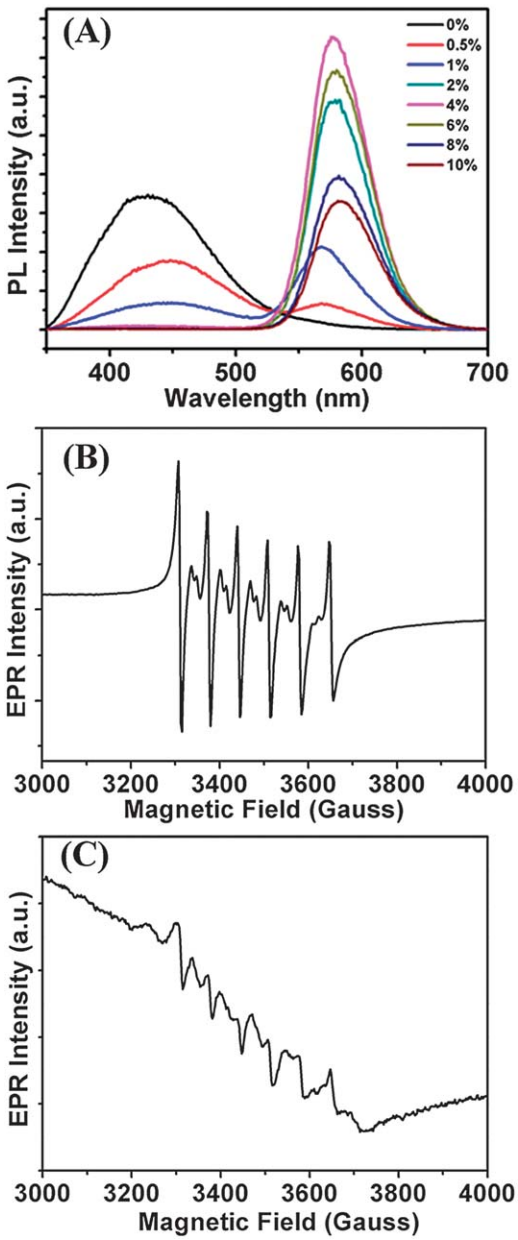


**Fig. 5** (A) PL spectra of the ZnS : Mn/ZnS core/shell d-dots with different Mn concentrations (nominal Mn/Zn molar ratios) in the preparation of the ZnS : Mn cores. EPR spectra of ZnS : Mn/ZnS core/shell d-dots with (B) 4% and (C) 10% Mn concentration, respectively.

surface of the QDs through the Zn–S. In addition, the IR absorption bands of the –COO groups (1600–1631 $cm^{-1}$, 1403 $cm^{-1}$) still existed in the prepared d-dots, indicating that GSH had capped the ZnS : Mn/ZnS core/shell d-dots. This result was also confirmed by the Raman spectra (Fig. S5†). The Raman band of the –SH stretching vibration at 2527 $cm^{-1}$ almost disappeared in the Raman spectra of GSH-capped ZnS : Mn/ZnS core/shell d-dots.[56]

### Influence of Mn doped concentration of ZnS host

The previous results indicated that the ZnS shell could be successfully deposited on the ZnS : Mn core, which improved the PL QY and consequently influenced the Mn emission position.[32–34] However, the Mn doped concentration was also a key factor for the PL property of the ZnS : Mn/ZnS core/shell d-dots. In order to study the influence of the Mn concentration on the PL property of the ZnS : Mn/ZnS core/shell d-dots, a series of ZnS : Mn cores doped with various Mn concentrations (from 0 to 10.0%, Mn/Zn molar ratios) were prepared in the first step, and then were deposited by ZnS shell under the identical conditions. PL emission spectra of the ZnS : Mn/ZnS core/shell d-dots prepared with different Mn doped concentrations were shown in Fig. 5A. The ZnS : Mn/ZnS d-dots without Mn doping showed a broad band emission around 430 nm which originated from the ZnS trap state. When the Mn was introduced into the ZnS cores, the characteristic $^4T_1$ to $^6A_1$ emission of $Mn^{2+}$ ions appeared *via* efficient energy transfer from ZnS host to the $Mn^{2+}$ ions. With the increase of the Mn doped concentration, the PL QY of the Mn emission increased, while the PL QY of the band emission decreased. The band emission totally disappeared when the Mn concentration reached 4.0%. The PL QY of the Mn emission reached a maximum of around 27.4% when the Mn concentration was 4.0% (Fig. 5A, Table S2†) and with

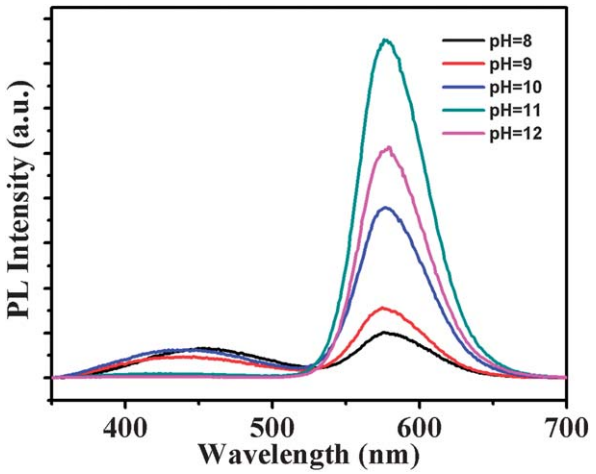


**Fig. 6** PL emission spectra of the ZnS : Mn/ZnS core/shell d-dots with different pH values.

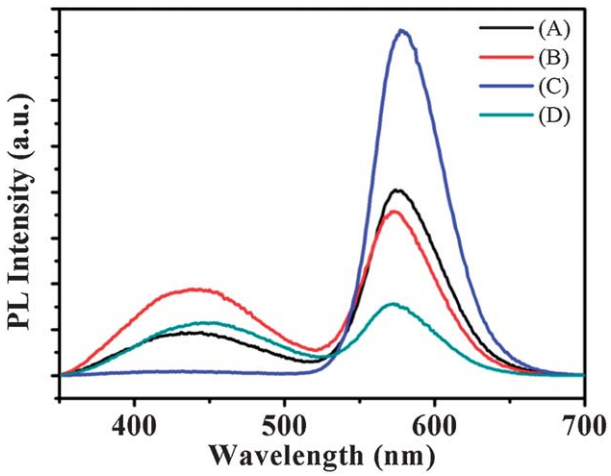


**Fig. 7** PL spectra of the ZnS : Mn/ZnS core/shell d-dots with different ligands (A) L-cys, (B) MPA, (C) GSH, (D) mercaptoethylamine.

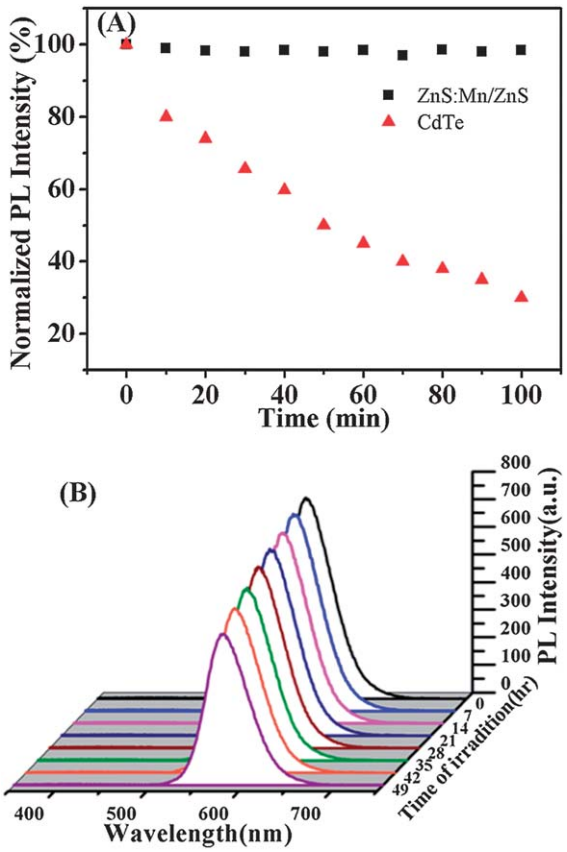


**Fig. 8** (A) Photostability comparison of ZnS : Mn/ZnS d-dots and CdTe QDs in aqueous solution under continuous irradiation at 260 nm source using a 150 W xenon lamp. (B) Photostability of the ZnS : Mn/ZnS d-dots under the same conditions but a longer irradiation time (panel A).

further increase of the Mn concentration, the PL QY of the Mn emission decreased.

The emission properties of $Mn^{2+}$ ions are closely related to the distribution of $Mn^{2+}$ ions in the doped QDs and the structure of the doped QDs. To confirm that the $Mn^{2+}$ ions are located inside the NCs, the EPR experiments were performed. Since the hyperfine splitting is strongly dependent on the local environment, EPR spectra can be used to determine the location of the Mn.[57,58] As shown in Fig. 5B, a hyperfine splitting of $64.4 \times 10^{-4}$ $cm^{-1}$ is observed, which is in agreement with that for internally $Mn^{2+}$-doped ZnS. The value of the hyperfine splitting constant for the Mn substituted at Zn sites in the cubic ZnS lattice was reported to be $64.0 \times 10^{-4}$ $cm^{-1}$.[51] The approximate value in our case indicated that the Mn was substitutionally incorporated into the ZnS host lattice. EPR spectroscopic characterization of ZnS : Mn/ZnS core/shell d-dots with 10% Mn concentration was observed in Fig. 5C. The broad line feature was the result of $Mn^{2+}$–$Mn^{2+}$ interactions within the ZnS lattice or $Mn^{2+}$ doped on the surface of ZnS. As a result, nonradiative decay of the Mn excited state increased, leading to a decreased PL QY of the Mn emission. Apart from the PL QY, the emission peak position also has been significantly influenced by the Mn concentration. A red shift of the Mn emission was observed clearly with the increase of the Mn doped concentration (Fig. 5A). The red shift of the Mn emission might be caused by the pair formation at higher doped concentrations, as reported in the literature.[59,60] As a result of magnetic interactions between neighboring $Mn^{2+}$ ions, the emission of magnetically coupled (ferromagnetic or antiferromagnetic) pairs was usually observed to be red-shift.

## Influence of pH on preparation of ZnS : Mn/ZnS core/shell d-dots

The pH of the reaction mixture is an extremely crucial factor for the synthesis of water-soluble quantum dots due to their influence on the densities of the reactants and stabilizers.[31,61,62] Fig. 6 shows the PL emission spectra of a series of ZnS : Mn/ZnS prepared with different pH (from 8.0 to 12.0) by using GSH as the ligand when fixing the Mn doped concentration ratio at 4%. Performing the PL emission spectra, as the pH value increased from 8.0 to 11.0, the PL intensity gradually increased, but when the pH value reached 12.0, the PL intensity decreased. There are three different coordination fashions of GSH with $Zn^{2+}$ under

 

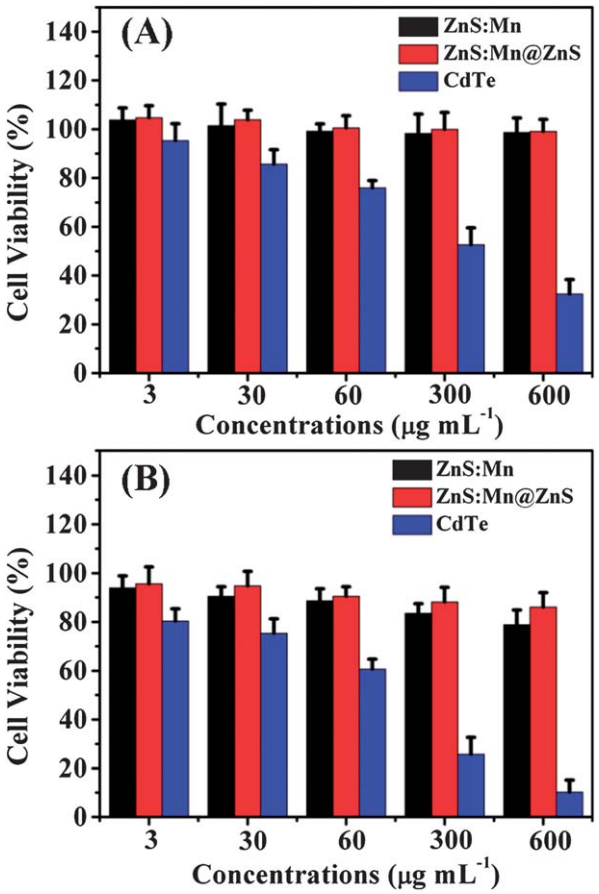


**Fig. 9** Cell viability in the presence of various concentrations of quantum dots for different incubation time: (A) 24 h; (B) 48 h.

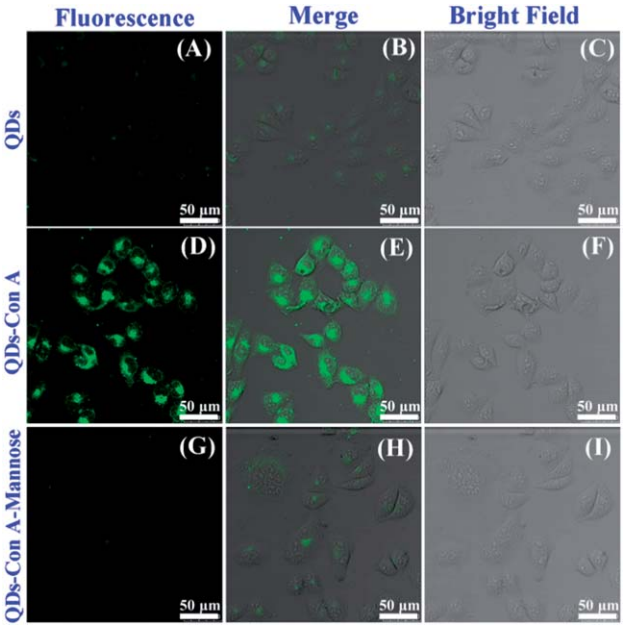


**Fig. 10** Specificity of ZnS : Mn/ZnS QDs-Con A probes for detecting the mannosyl groups on the HeLa cells surface. (A)–(C) ZnS : Mn/ZnS QDs alone, (D)–(F) ZnS : Mn/ZnS QDs-Con A conjugate, (G)–(I) ZnS : Mn/ZnS QD-Con A-mannose. Scale bar: 50 μm. Under the same procedure, there were no detectable emissions from the control cells. The green color in all confocal images was a pseudocolor.

different pH values according to ref. 63 (Fig. S6†). It is identified that $Zn^{2+}$ primarily coordinates with thiol group of the cysteine residual at low pH (6.5–8.3); then, the deprotonated amino group of the glutamyl residue also contributed to the coordination at medium pH (8.3–10.3). By increasing the pH to greater than 10.3, in ZnS : Mn/ZnS, the N atom of the amide bond took part in the coordination after its deprotonation. As a result, the growth rate of the ZnS : Mn/ZnS NCs increased with increasing pH, indicating the improved activity of the $Zn^{2+}$ precursors with increased pH. When the pH values increased further to 12, the PL intensity decreased. The existence of a large excess of OH ions might cause the formation of the manganese oxide or manganese hydroxide or zinc oxide, which had a disastrous influence on the PL QY.

### Influence of the various ligands

The effect of various thiols (GSH, MPA, L-cys, and mercaptoethylamine) on the PL of ZnS : Mn d-dots was investigated when the $Zn^{2+}/S^{2-}$/ligand molar ratio and the doping percentage were fixed at the same conditions (Fig. 7). GSH, MPA, L-cys and mercaptoethylamine-capped ZnS : Mn d-dots exhibited the $Mn^{2+}$ $^4T_1$ to $^6A_1$ transition at about ~580 nm. The PL QYs of Mn emission of the NCs prepared with MPA, L-cys and mercaptoethylamine were found to be weaker than those of GSH as the capping ligand. The nanocrystal growth with mercaptoethylamine, MPA and L-cys ligands occurred with higher defect densities eventually (increase of the ZnS band-edge transition at about 430 nm). Jin's group reported that ligands with electron-rich atoms (*e.g.* N, O) or groups (*e.g.* –COOH, $NH_2$) can largely promote the fluorescence of nanoparticles.[64] Compared to MPA, L-cys and mercaptoethylamine, each glutathione molecule contains both amine and carboxyl groups, which provide more coordination possibilities with $Zn^{2+}$ and improve the fluorescence of ZnS : Mn d-dots. We suggest that GSH provides better surface passivation of the QD crystalline lattice under our synthetic conditions.

### Stability of ZnS : Mn/ZnS core/shell d-dots

High PL QY and good photostability were prerequisites of d-dots in numerous applications. Thus, the photostability of the obtained core/shell d-dots was also investigated. The photostability study was carried out by continuously irradiation under a 260 nm source provided by a 150 W xenon lamp, with CdTe QDs[54] as a control. The PL emission spectra of both the ZnS : Mn/ZnS core/shell d-dots and CdTe QDs were monitored. As shown in Fig. 8, it can be clearly observed that, the PL emission of the CdTe QDs became unstable and decreased to 30% of the original PL intensity after 100 min intense UV irradiation. In striking contrast, ZnS : Mn/ZnS core/shell d-dots displayed excellent photostability during the whole 100 min UV irradiation. The long-term investigation found that the PL intensity of the ZnS : Mn/ZnS core/shell d-dots remained at 93% after 35 h and 75% after 49 h of irradiation, respectively (Fig. 8B). In addition, the ZnS : Mn/ZnS QDs could keep stability

over 48 h in the pH range of 4.5–8.5 under biologically relevant conditions (Fig. S7†). Moreover, a white powder was obtained by precipitating the ZnS : Mn/ZnS QDs with ethanol and drying under vacuum at room temperature. The solid of ZnS : Mn/ZnS QDs emitted strong luminescence and were found to be stable for at least one year under normal atmospheric conditions (Fig. S8†). The excellent photostability of ZnS : Mn/ZnS core/shell d-dots may be attributed to the nature of the internal electronic transition of the Mn ($^4T_1$ to $^6A_1$) and noncoupling with the lattice phonons.

### Cytotoxicity evaluation

Generally, the actual biological application of QDs needs to address the question about their biocompatibility. Low or no cytotoxicity is one of the most critical parameters for ideal biomaterials. To evaluate the cytotoxicity of our as-prepared GSH-capped ZnS : Mn d-dots, the MTT assay was introduced. Fig. 9 displays the cell viability of the HeLa cells in the presence of CdTe QDs, ZnS : Mn d-dots and ZnS : Mn/ZnS core/shell d-dots. In the case of CdTe, only 32.5% and 10.3% of cells survived after incubation with 600 μg $mL^{-1}$ CdTe QDs for 24 h and 48 h, respectively. In contrast, ZnS : Mn d-dots and ZnS : Mn/ZnS core/shell d-dots exhibited much lower cytotoxicity than CdTe QDs (greater than 80% cell viability) and the viability was slightly affected even at the concentrations as high as 600 μg $mL^{-1}$ for 48 h. These data suggest the promising potential of these ZnS : Mn d-dots as robust biomarkers due to their good biocompatibility.

### Fluorescence imaging for the mannosyl group

To further investigate the performance of the ZnS : Mn/ZnS QDs for bio-imaging and nano-diagnostics, Con A, with a specific and high affinity to mannose,[65,66] was linked to the ZnS : Mn/ZnS QDs *via* NHS/EDC chemistry to fabricate a fluorescence probe for detecting the mannosyl groups overexpressed on HeLa cell surfaces. As illustrated in Fig. 10D–F, the HeLa cells treated with ZnS : Mn/ZnS QDs-Con A (QDs-Con A) showed strong fluorescence, indicating that the QDs-Con A can efficiently target the cell surface mannosyl groups. In comparison, a weak fluorescence was observed for the cells treated with bare QDs (Fig. 10A–C) due to nonspecific adsorption. To further validate the role of the Con A in cell labeling, a control assay was performed by treating QDs-Con A with excess of mannose solution to block the recognition sites of Con A. Owing to the blocking of mannose-specific binding sites, the amount of QDs-Con A targeted to the mannosyl groups on cell surfaces decreased, resulting in a drastic decrease in fluorescence intensity compared to that obtained without blocking (Fig. 10G–I). More importantly, no sign of morphological damage to the cells was observed upon incubation with the ZnS : Mn/ZnS QDs which further demonstrated their low cytotoxicity. This result indicates that the ZnS : Mn/ZnS QDs could become a potential material for biological application.

## Conclusions

In summary, we have developed a simple effective method for producing GSH-capped ZnS : Mn NCs and core/shell ZnS : Mn/ZnS QDs with pure dopant emissions *via* aqueous phase and low-temperature transition metal doping. By rationally tailoring the experimental parameters, the highly luminescent ZnS : Mn/ZnS d-dots with core/shell structure were obtained. The as-prepared ZnS : Mn/ZnS core/shell d-dots possessed excellent stability and low cytotoxicity. Compared with the traditional synthetic methods for d-dots, our method required only low-cost and nontoxic chemicals under mild conditions. Because of the excellent optical properties observed, it is expected that these water-dispersible and non-cadmium ZnS : Mn/ZnS NCs will be promising candidates for the nanoprobes in bio-imaging and nano-diagnostics.

## Acknowledgements

We gratefully appreciate the grants of the National Natural Science Foundation (21175065 and 21121091) and the National Basic Research Program (2011CB933502) of China.

## References

1 M. Bruchez Jr and M. Moronne, *Science*, 1998, **281**, 2013.
2 S. Coe, W. K. Woo, M. Bawendi and V. Bulović, *Nature*, 2002, **420**, 800.
3 Q. Sun, Y. A. Wang, L. S. Li, D. Y. Wang, T. Zhu, J. Xu, C. H. Yang and Y. F. Li, *Nat. Photonics*, 2007, **1**, 717–722.
4 N. Hildebrandt, *ACS Nano*, 2011, **5**, 5286–5290.
5 P. K. Santra and P. V. Kamat, *J. Am. Chem. Soc.*, 2012, **134**, 2508–2511.
6 L. Li, Y. Cheng, Y. P. Ding, Y. X. Lu and F. F. Zhang, *Anal. Methods*, 2012, **4**, 4213–4219.
7 Y. T. Long, C. Kong, D. W. Li, Y. Li, S. Chowdhury and H. Tian, *Small*, 2011, **7**, 1624–1628.
8 X. G. Peng, L. Manna, W. D. Yang, J. Wickham, E. Scher, A. Kadavanich and A. P. Alivisatos, *Nature*, 2000, **404**, 59–61.
9 Y. F. Chen, T. H. Ji and Z. Rosenzweig, *Nano Lett.*, 2003, **3**, 581–584.
10 Y. Zheng, Z. Yang and J. Y. Ying, *Adv. Mater.*, 2007, **19**, 1475–1479.
11 G. X. Liang, L. L. Li, H. Y. Liu, J. R. Zhang, C. Burda and J. J. Zhu, *Chem. Commun.*, 2010, **46**, 2974–2976.
12 T. E. Rosson, S. M. Claiborne, J. R. McBride, B. S. Stratton and S. J. Rosenthal, *J. Am. Chem. Soc.*, 2012, **134**, 8006–8009.
13 Y. Shen, L. Li, Q. Lu, J. Ji, R. Fei, J. Zhang, E. S. Abdel Halim and J. J. Zhu, *Chem. Commun.*, 2012, **48**, 2222–2224.
14 W. Ma, L. X. Qin, F. T. Liu, Z. Gu, J. Wang, Z. G. Pan, T. D. James and Y. T. Long, *Sci. Rep.*, 2013, **3**.
15 C. Kirchner, T. Liedl, S. Kudera, T. Pellegrino, A. M. Javier, H. E. Gaub, S. Stolzle, N. Fertig and W. J. Parak, *Nano Lett.*, 2005, **5**, 331–338.
16 D. J. Norris, A. L. Efros and S. C. Erwin, *Science*, 2008, **319**, 1776–1779.
17 D. Mocatta, G. Cohen, J. Schattner, O. Millo, E. Rabani and U. Banin, *Science*, 2011, **332**, 77–81.
18 P. Wu and X. P. Yan, *Chem. Soc. Rev.*, 2013, **42**, 5489–5521.
19 N. Pradhan and X. Peng, *J. Am. Chem. Soc.*, 2007, **129**, 3339–3347.

 

20 N. Pradhan and D. D. Sarma, *J. Phys. Chem. Lett.*, 2011, **2**, 2818–2826.
21 D. J. Norris, N. Yao, F. T. Charnock and T. A. Kennedy, *Nano Lett.*, 2000, **1**, 3–7.
22 A. Sahu, M. S. Kang, A. Kompch, C. Notthoff, A. W. Wills, D. Deng, M. Winterer, C. D. Frisbie and D. J. Norris, *Nano Lett.*, 2012, **12**, 2587–2594.
23 D. Zhu, X. Jiang, C. Zhao, X. Sun, J. Zhang and J. J. Zhu, *Chem. Commun.*, 2010, **46**, 5226–5228.
24 R. Zeng, M. Rutherford, R. Xie, B. Zou and X. Peng, *Chem. Mater.*, 2010, **22**, 2107–2113.
25 J. Zheng, W. Ji, X. Wang, M. Ikezawa, P. Jing, X. Liu, H. Li, J. Zhao and Y. Masumoto, *J. Phys. Chem. C*, 2010, **114**, 15331–15336.
26 C. H. Hsia, A. Wuttig and H. Yang, *ACS Nano*, 2011, **5**, 9511–9522.
27 B. Thi Luong, E. Hyeong, S. Ji and N. Kim, *RSC Adv.*, 2012, **2**, 12132–12135.
28 M. Geszke, M. Murias, L. Balan, G. Medjahdi, J. Korczynski, M. Moritz, J. Lulek and R. Schneider, *Acta Biomater.*, 2011, **7**, 1327–1338.
29 H. Wu and Z. F. Fan, *Spectrochim. Acta, Part A*, 2012, **90**, 131–134.
30 Y. He, H. F. Wang and X. P. Yan, *Anal. Chem.*, 2008, **80**, 3832–3837.
31 J. Zhuang, X. Zhang, G. Wang, D. Li, W. Yang and T. Li, *J. Mater. Chem.*, 2003, **13**, 1853–1857.
32 W. Jian, J. Zhuang, W. Yang and Y. Bai, *J. Lumin.*, 2007, **126**, 735–740.
33 Q. Xiao and C. Xiao, *Opt. Mater.*, 2008, **31**, 455–460.
34 J. Zheng, X. Yuan, M. Ikezawa, P. Jing, X. Liu, Z. Zheng, X. Kong, J. Zhao and Y. Masumoto, *J. Phys. Chem. C*, 2009, **113**, 16969–16974.
35 B. B. Srivastava, S. Jana, N. S. Karan, S. Paria, N. R. Jana, D. D. Sarma and N. Pradhan, *J. Phys. Chem. Lett.*, 2010, **1**, 1454–1458.
36 S. Q. Chang, B. Kang, Y. D. Dai, H. X. Zhang and D. Chen, *Nanoscale Res. Lett.*, 2011, **6**, 591–598.
37 W. Zhang, Y. Li, H. Zhang, X. Zhou and X. Zhong, *Inorg. Chem.*, 2011, **50**, 10432–10438.
38 R. Begum, S. Bhandari and A. Chattopadhyay, *Langmuir*, 2012, **28**, 9722–9728.
39 W. Y. Xie, W. T. Huang, H. Q. Luo and N. B. Li, *Analyst*, 2012, **137**, 4651–4653.
40 H. Yan and H. F. Wang, *Anal. Chem.*, 2011, **83**, 8589–8595.
41 H. F. Wang, Y. Li, Y. Y. Wu, Y. He and X. P. Yan, *Chem.–Eur. J.*, 2010, **16**, 12988–12994.
42 M. Geszke Moritz, H. Piotrowska, M. Murias, L. Balan, M. Moritz, J. Lulek and R. Schneider, *J. Mater. Chem. B*, 2013, **1**, 698–706.
43 L. Cao, J. Zhang, S. Ren and S. Huang, *Appl. Phys. Lett.*, 2002, **80**, 4300–4302.
44 D. Jiang, L. Cao, W. Liu, G. Su, H. Qu, Y. Sun and B. Dong, *Nanoscale Res. Lett.*, 2008, **4**, 78–83.
45 Y. T. Nien, K. H. Hwang, I. G. Chen and K. Yu, *J. Alloys Compd.*, 2008, **455**, 519–523.
46 D. Jiang, L. Cao, G. Su, H. Qu and D. Sun, *Appl. Surf. Sci.*, 2007, **253**, 9330–9335.
47 I. Chakraborty, U. B. R. Thumu and T. Pradeep, *Chem. Commun.*, 2012, **48**, 6788–6790.
48 J. Du, X. Li, S. Wang, Y. Wu, X. Hao, C. Xu and X. Zhao, *J. Mater. Chem.*, 2012, **22**, 11390–11395.
49 C. T. Chen, W. J. Chen, C. Z. Liu, L. Y. Chang and Y. C. Chen, *Chem. Commun.*, 2009, 7515–7517.
50 H. Lis and N. Sharon, *Chem. Rev.*, 1998, **98**, 637–674.
51 W. H. Melhuish, *J. Phys. Chem.*, 1961, **65**, 229–235.
52 M. Grabolle, M. Spieles, V. Lesnyak, N. Gaponik, A. Eychmuller and U. Resch Genger, *Anal. Chem.*, 2009, **81**, 6285–6294.
53 S. H. Liu, F. Lu, X. d. Jia, F. Cheng, L. P. Jiang and J. J. Zhu, *CrystEngComm*, 2011, **13**, 2425–2429.
54 A. L. Rogach, T. Franzl, T. A. Klar, J. Feldmann, N. Gaponik, V. Lesnyak, A. Shavel, A. Eychmuller, Y. P. Rakovich and J. F. Donegan, *J. Phys. Chem. C*, 2007, **111**, 14628–14637.
55 P. Wu, L. N. Miao, H. F. Wang, X. G. Shao and X. P. Yan, *Angew. Chem., Int. Ed.*, 2011, **50**, 8118–8121.
56 Z. Ke, Z. Yu and Q. Huang, *Plasma Processes Polym.*, 2013, **10**, 181–188.
57 T. A. Kennedy, E. R. Glaser, P. B. Klein and R. N. Bhargava, *Phys. Rev. B: Condens. Matter Mater. Phys.*, 1995, **52**, R14356–R14359.
58 P. A. Gonzalez Beermann, B. R. McGarvey, S. Muralidharan and R. C. W. Sung, *Chem. Mater.*, 2004, **16**, 915–918.
59 Z. Fang, P. Wu, X. H. Zhong and Y. J. Yang, *Nanotechnology*, 2010, **21**, 305604–305612.
60 B. Dong, L. Cao, G. Su and W. Liu, *J. Phys. Chem. C*, 2012, **116**, 12258–12264.
61 F. Zhang, X. W. He, W. Y. Li and Y. Zhang, *J. Mater. Chem.*, 2012, **22**, 22250–22257.
62 D. Zhao, Z. He, W. H. Chan and M. M. F. Choi, *J. Phys. Chem. C*, 2008, **113**, 1293–1300.
63 J. Zhang, J. Li, J. Zhang, R. Xie and W. Yang, *J. Phys. Chem. C*, 2010, **114**, 11087–11091.
64 Z. Wu and R. Jin, *Nano Lett.*, 2010, **10**, 2568–2573.
65 J. T. Cao, Z. X. Chen, X. Y. Hao, P. H. Zhang and J. J. Zhu, *Anal. Chem.*, 2012, **84**, 10097–10104.
66 F. F. Cheng, G. X. Liang, Y. Y. Shen, R. K. Rana and J. J. Zhu, *Analyst*, 2013, **138**, 666–670.